The pyrolysis behavior and biochar characteristics of Jerusalem artichoke straw with cerium nitrate

Lu Wang [a, b], Gaigai Xue [a], Ting Li [a], Tao Ye [a], Xianming Ma [a], Xiaohui Ju [c], Peiyong Ma [d], Jian Liu [a, *], Hanwu Lei [e, *]

[a] School of Food and Biological Engineering, Hefei University of Technology, Hefei, Anhui, 230009, China.

[b] Engineering Research Center of Bio-process, Ministry of Education, Hefei University of Technology, Hefei, 230009, China.

[c] Department of Surface and Plasma Science, Faculty of Mathematics and Physics, Charles University, Prague, 18 000, Czech Republic.

[d] School of Mechanical Engineering, Hefei University of Technology, Hefei, Anhui, 230009, China.

[e] Bioproducts, Sciences and Engineering Laboratory, Department of Biological Systems Engineering, Washington State University, Richland, WA 99354-1671, USA.

* Corresponding authors at:

Bioproducts, Sciences and Engineering Laboratory, Department of Biological Systems Engineering, Washington State University, Richland, WA 99354-1671, USA. Tel.: +1 509 3727628

School of Food and Biological Engineering, Hefei University of Technology, Hefei, 230009, Anhui, P. R. China. Tel.: +86 551 62919398

E-mail addresses: hlei@wsu.edu (H. Lei); liujian509@hfut.edu.cn (J. Liu).

Abstract

The pyrolysis behavior of Jerusalem artichoke straw with cerium nitrate was analyzed by thermogravimetric analyzer coupled with Fourier-transform infrared spectroscopy. Then the cerium oxide doped biochar was obtained from the pyrolysis of Jerusalem artichoke straw impregnated with cerium nitrate. And the electrochemical characteristics and physical structures of the cerium oxide doped biochar from different pyrolysis temperature were analyzed. TG results showed that the addition of cerium nitrate reduced the reaction energy and pyrolysis temperature, facilitating the pyrolysis reaction. FTIR results revealed that H_2O, CO_2, CO, CH_4, C-O, C=O and aromatic C=C were released during the pyrolysis. The cyclic voltammetry curves of the electrode modified with cerium oxide doped biochar indicated that the biochar derived from higher pyrolysis temperature showed better enhancing effect for electrochemical properties. Nanostructured cerium oxide was observed on the surface rather than in the pores of biochar. The existence of a crystallite structure with a mixture of Ce^{3+}/Ce^{4+} oxidation states further confirmed the formation of nanostructured cerium oxide. The finding revealed that cerium oxide doped biochar composites demonstrates the potential for a wide application in electrochemistry.

Keywords: Jerusalem artichoke; cerium oxide; biochar; pyrolysis; electrochemistry.

1. Introduction

Disadvantages of non-renewable resources, such as high energy consumption cost, enormous environmental pollution, and excessive gas emissions, motivate people to research and use renewable and sustainable biomass resources [1]. Jerusalem artichoke, Helianthus of the composite family, annual herbs, originated from North America, is one of the promising energy crops [2]. Compared

with other crops, Jerusalem artichokes have the advantages of a fast growth rate, wide adaptability, and big biomass [3]. The Jerusalem artichoke tuber is rich in inulin, which can be converted into bioethanol efficiently and has wide application in medical and functional foods [4], while Jerusalem artichoke stalk and leaves are often used for cooking or just heating, which may cause environmental pollution and waste of resource.

Jerusalem artichoke stalk and leaves can be transformed into renewable energy through thermochemical progress, for example, pyrolysis, combustion, torrefaction, gasification, and liquefaction [5]. Pyrolysis is appealing because its products (synthetic gas, biochar, and bio-oil) could be used as energy [6]. Biochar is a solid product of biomass pyrolysis under oxygen-free conditions, which is produced from plant residues, animal feces, and sewage sludge [7]. Biochar has a porous structure, high surface area, and abundant functional groups, making it a potential material to remove liquid or gas pollutants [8], store energy [9], improve soil quality [10], and accelerate reaction rates [11].

Modification of biochar is attractive because it can improve biochar's performance and expand biochar's application [8]. Cerium oxide modified biochar has been extensively studied in recent years due to its superior performance as a catalyst. For example, maize straw impregnation with $CeCl_3$ was used to prepare cerium oxide modified biochar through pyrolysis to remove phosphorus from wastewater [12]. There has been report of using hydrothermal method to prepare the cerium oxide modified biochar composite with enhanced sonic catalytic efficiency on removal of RR18 compared with single component [13]. Several metals (Fe, Ce, La, Al, Ti) were selected to modify the sludge to obtain biochar with high catalytic capacity. More metal oxide was found in biochar with extensive modification of surface morphology and increased amounts of structural defects. Both Ce^{3+} and Ce^{4+}

oxidations states were observed, indicating cerium oxide formation. Cerium oxide doped biochar exhibited better catalytic degradation of tetracycline than Fe modified biochar [14].

The physicochemical properties of biochar are usually influenced by the type of the raw materials, the pyrolysis temperatures during the modification. Among these parameters, pyrolysis temperatures could significantly impact the final elemental composition, functional groups, and surface roughness of biochar [15]. It was reported that with the increase in pyrolysis temperature, the amount of surface functional groups decreased, and the surface-specific area and iron content were improved. γ-Fe_2O_3 loaded on the biochar was transformed to Fe_3O_4 when pyrolysis temperatures increased from 400 to 600 ℃ [16]. Cu^{2+} polluted cotton leaf was recycled to prepare Cu-contained biochar through pyrolysis at different temperatures. It was observed that when pyrolysis temperatures were 350, 550, and 750 ℃, Cu existed in Cu^{2+}, Cu^{2+}/Cu^{1+}/Cu, and Cu. With the elevated pyrolysis temperatures, the sizes of Cu decreased [17]. In our previous work [18], 3D porous carbon-loaded cerium nanoparticles were prepared by in-situ pyrolysis of cerium nitrate pretreated Jerusalem artichoke straw biomass, and had excellent electrochemical catalytic oxidation ability. However, the relationship between the pyrolysis process and the physicochemical properties of cerium modified biochar remains unclear.

Therefore, the aim of this study was to analyze the relationship of pyrolysis process of cerium nitrate impregnated Jerusalem artichoke straw (JAC/Ce) with the physicochemical properties of cerium oxide doped Jerusalem artichoke straw biochar (JAC/Ce-BC), and thereby to demonstrate the electrochemical potential of JAC/Ce-BC. Frist, the kinetics of thermal decomposition of JAC/Ce was studied by thermogravimetric analyzer coupled with Fourier-transform infrared spectroscopy (TG-FTIR). Then JAC/Ce-BC was prepared by pyrolysis and the electrochemical catalytic activity of JAC/Ce-BC was evaluated through cyclic voltammetry (CV). Finally, the structure and components

of JAC/Ce-BC were analyzed through characterization such as Scanning electron microscope (SEM), Energy Dispersive Spectrometer (EDS), X-ray diffraction (XRD), Raman and X-ray photoelectron spectroscopy (XPS) and showed that JAC/Ce-BC had better electrochemical performance.

2. Material and methods

2.1 Materials

Jerusalem artichoke used in this study was collected from Hefei, Anhui. Before the experiment, the Jerusalem artichoke was washed with water to eliminate impurities and mud, then dried at 105 ℃ overnight to remove moisture. After drying, the straw and core of Jerusalem artichoke were separated and stored separately. Jerusalem artichoke straw core was ground by a high-speed multi-functional mill and marked as JAC. 300 mL cerium nitrate solution (2 mM) was mixed with a certain amount of JAC under continuous stirring for two hours. After that, the solid was separated from the solution by suction filtration. The solid was dried at 65 ℃ overnight and marked as JAC/Ce.

Phosphate buffered saline (10 × PBS, pH = 7.4) was purchased from Sangon (Shanghai, China). Cerium nitrate hexahydrate (Cerium nitrate·$6H_2O$) was purchased from Macklin (Shanghai, China). Hydrogen peroxide (H_2O_2) and Chitosan (CS) were purchased from Sinopharm (Shanghai, China). Ultrapure deionized (DI) water was produced by a Milli-Q system (18.2 MΩ, Millipore, Bedford, MA, USA). All the reagents were used without further purification.

2.2 Thermal behavior analysis

Thermogravimetric analyzer (TG, STA409C/3/F, German) and Fourier transform infrared spectrometry (FT-IR, Nexus 670, American) were combined to analyze gas products during pyrolysis. Approximately 10 mg of sample was loaded onto the sample holder. The samples were heated from

30 to 600 ℃ at a heating rate of 10 ℃·min^{-1}. The carrier gas flow rate (high purity nitrogen) was 100 mL^{-1}·min^{-1}.

2.3 Calculation of kinetic parameters

In this study, the mass loss of samples can be expressed as Eq. (1)

$$\alpha = \frac{m_0 - m_t}{m_0 - m_f} \quad (1)$$

where α is the conversion rate, m_0 is the initial mass of the sample, m_t is the mass of the sample at time t, m_f is the final mass of the sample.

Arrhenius equation was used to describe the pyrolysis process of TG:

$$\frac{d\alpha}{dt} = k(T)f(\alpha) \quad (2)$$

$$k(T) = Aexp\left(-\frac{E}{RT}\right) \quad (3)$$

A is a pre-exponential factor (min^{-1}), E presents apparent activation energy (kJ), R is the universal gas constant (8.314 J·mol^{-1}·K^{-1}), T is the absolute temperature (K), and f(α) is the mechanism function that represents the reaction model.

Heating rate $\frac{dT}{dt}$ was denoted as β, integrated it with Eq. (2) and Eq. (3)

$$\beta\frac{d\alpha}{dT} = Aexp(-\frac{E}{RT})f(\alpha) \quad (4)$$

Assume that $g(\alpha) = \int_0^\alpha \frac{d\alpha}{f(\alpha)}$, combine the aforementioned three equations:

$$g(\alpha) = \int_0^\alpha \frac{d\alpha}{f(\alpha)} = \frac{A}{\beta}\int_{T_0}^{T} \exp(-\frac{E}{RT})dT \quad (5)$$

The coats-Redfern method was selected to fit the reaction model of sample pyrolysis because it needs only one heating rate. The form of the Coats-Redfern method was based on a first-order reaction.

when n=1,

$$\ln(\frac{-\ln(1-\alpha)}{T^2}) = \ln\frac{AR}{\beta E} - \frac{E}{RT} \quad (6)$$

When n≠1,

$$\ln\left(\frac{1-(1-\alpha)^{1-n}}{T^2(1-n)}\right) = \ln\frac{AR}{\beta E} - \frac{E}{RT} \quad (7)$$

2.4 Preparation of biochar from cerium nitrate impregnated Jerusalem artichoke straw core

The pyrolysis of JAC and JAC/Ce were carried out in a tubular furnace. Before pyrolysis, nitrogen gas was flushed in for 30min in order to discharge air. Then JAC or JAC/Ce was heated to the required temperature (400, 600 and 800 ℃) with a heating rate at 10 ℃·min^{-1}, and a residence time of 120 min. After cooling down to room temperature, biochar was collected and cleaned with ethanol and water. The biochar of JAC and JAC/Ce were labeled as JAC-BC and JAC/Ce-BC. Based on the different pyrolysis temperature, JAC-BCs were denoted as JAC-BC 400, JAC-BC 600 and JAC-BC 800. And JAC/Ce-BCs were denoted as JAC/Ce-BC 400, JAC/Ce-BC 600 and JAC/Ce-BC 800.

2.5 Electrochemical measurement

The cleaned JAC/Ce-BC was dispersed in acetic acid (1%) - chitosan solution (20 mg·100mL^{-1}) and configured into a 1 mg·mL^{-1} mixture to modify the gold electrode, which was allowed to dry naturally at room temperature. Cyclic voltammetry was performed at a conventional electrochemical workstation (platinum wire as the auxiliary electrode, saturated calomel electrode as the reference electrode, and bare or modified gold electrode as the working electrode), and CV was measured in 1× PBS buffer containing 10 mM, with a potential range of 0-0.8 V and a scan rate of 50 mV·s^{-1}.

2.6 Biochar characterization

The morphology of the biochar was observed by field emission scanning electron microscopy (FE-SEM, Gemini SEM 500, Germany). EDS coupled with FE-SEM was used to detect the distribution of elements on the surface. The crystalline structure of the biochar was studied by X-ray

diffractometer (XRD, X'Pert Pro MPD, Netherlands) collected from 10 to 60 ° with a Cu target (40 kV, 40 mA). The chemical states of the elements were obtained by X-ray photoelectron spectroscopy (XPS, ESCALAB 250, USA). The degree of structure defect was characterized using a fully automatic Raman spectrometer (Raman, LabRAM HR, France) with a 633 nm wavelength laser.

3. Result and discussion

3.1 Thermal degradation behavior and kinetics analysis

As shown in Fig. 1(a, b), the decomposition process of JAC and JAC/Ce could be divided into three stages: the first stage was the evaporation of water, starting from 30 to 121 ℃; the second stage was between 121 and 400 ℃ with that carbohydrate (mainly hemicellulose and cellulose) decomposing into small molecular-weight matters. After temperatures exceed 400 ℃ (up to 618 ℃), lignin converts into char in the third stage [1]. A different process between JAC and JAC/Ce were observed from DTG curves. The DTG curves of JAC/Ce had a shoulder peak before 300 ℃, which might be from the decomposition of cerium nitrate.

Activation energy (EA) was calculated by Coats-Redfern method according to Eq. (5) and (6), and the linear fitting was shown in Fig. 1(c) and the results were shown in Table 1. As shown in Fig. 1(c), the linear fit effect for pyrolysis of JAC and JAC/Ce best, which was confirmed with Relatively high R values. When n=1, The E_A calculated from JAC and JAC/Ce were 58.351 kJ and 50.715 kJ, respectively. The addition of cerium nitrate decreased the E_A of reactions, which could reduce the pyrolysis temperature and make the pyrolysis reaction easier [19].

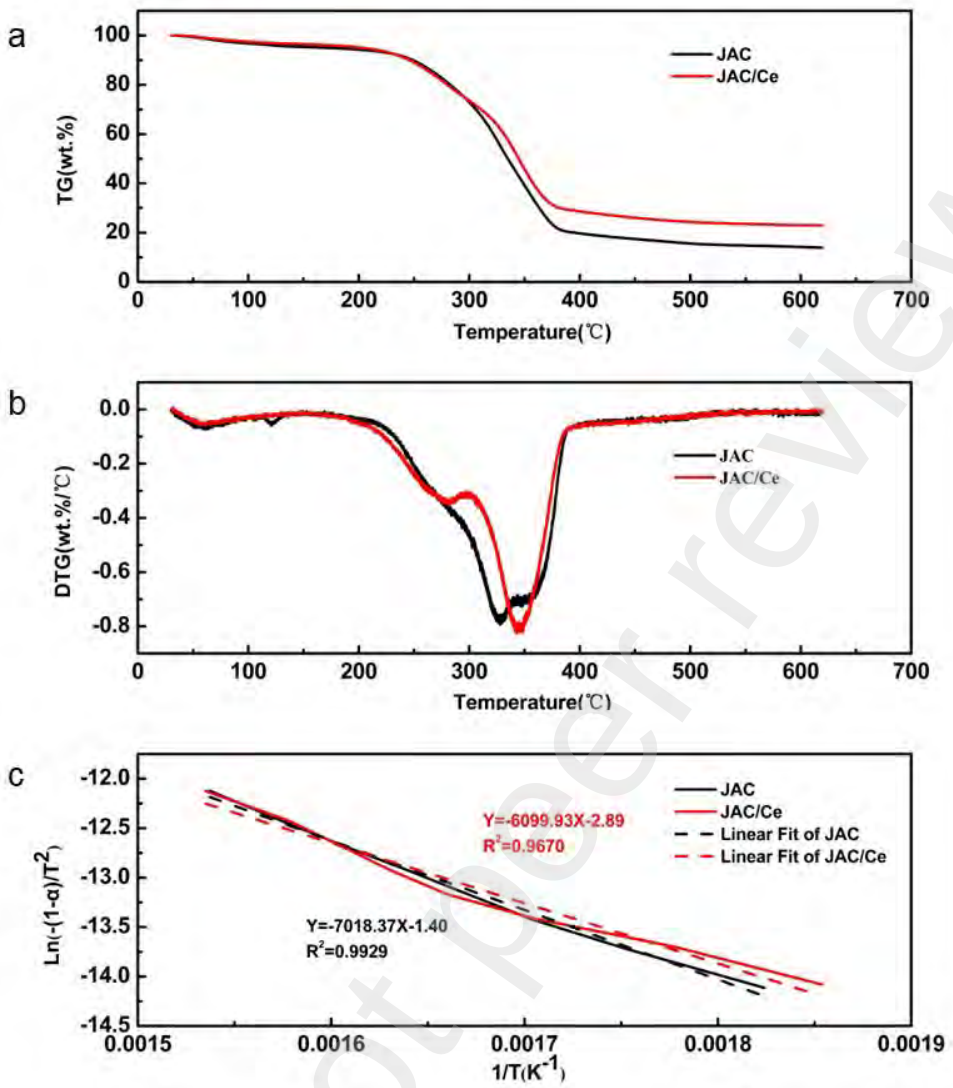

Fig. 1. TG (a) and DTG(b) curves of JAC and JAC/Ce. Coats-Redfern(c) model of JAC and JAC/Ce.

Table 1 E_A and R^2 of JAC and JAC/Ce yielded by the Coats-Redfern method.

Feedstock	JAC		JAC/Ce	
n	E_A (kJ)	R^2	E_A (kJ)	R^2
1	58.35	0.9939	50.71	0.9717
2	91.93	0.9568	79.73	0.9175
3	134.07	0.9172	116.08	0.87

3.2 TG-FTIR analysis

As shown in Fig. 2, three temperature points (278, 330, and 550 ℃) were selected to study the volatiles released during JAC and JAC/Ce pyrolysis by TG-FTIR. The absorbance peak between 4000 ~ 3500 cm^{-1} was ascribed to the vibration of the O-H bond in H_2O. The results showed that the water yield of JAC and JAC/Ce increased with the temperature from 278 to 330 ℃, and reached the maximum at 330 ℃, which might be caused by ring opening, depolymerization, recondensation and repolymerization at higher temperature [20,21].

The absorbance peak between 3050 and 2800 cm^{-1} represented C-H bond in saturated hydrocarbon alkyl, and the main substance was CH_4. The CH_4 gas generated by JAC and JAC/Ce both increased with the increase of temperature, and reached the highest value at 330 ℃, which was mainly related to the side chain break of saturated hydrocarbons and the demethylation of methoxy groups in some compounds during the pyrolysis process [2,22-24].

The significant peaks appeared at 660 cm^{-1} and 2358 cm^{-1} were corresponded to CO_2 absorption peaks. The production of CO_2 from JAC reached the maximum at 330 ℃, and keep on release till 550 ℃, indicating that the pyrolysis of JAC was not completed at 550 ℃. For JAC/Ce, the release of CO_2 reached the highest at 278 ℃ and showed a continuous downward trend, while almost no CO_2 was released at 550 ℃, indicating that cerium nitrate accelerated the pyrolysis rate of JAC.

The absorption peak of CO appeared at 2180 ~ 2100 cm^{-1}, which was more obvious at 330 ℃. This might be due to the incomplete combustion of C, or the reduction reaction of CO_2 with coke [25,26]. The stretching vibration of the adsorption band were C=O and C-O in 1780 ~ 1750 cm^{-1} and 1260 ~ 1000 cm^{-1}, respectively. This might be due to the acids, ketones, aldehydes, esters and furans compounds from the breaking and recombination during the pyrolysis of JAC and JAC/Ce [25,27].

The absorption peak at 1500 cm^{-1} might be caused by stretching vibration of aromatic C=C [28].

The formation of C=C might be related to β-hydrogen ester and cinnamyl diester during pyrolysis [2]. For JAC, the absorption peak of C=C began to appear when the temperature increased from 278 to 330 ℃, while the JAC/Ce had an obvious absorption peak from 278 ℃. This indicated that the addition of cerium nitrate reduced the initial pyrolysis temperature and accelerated the pyrolysis process [29].

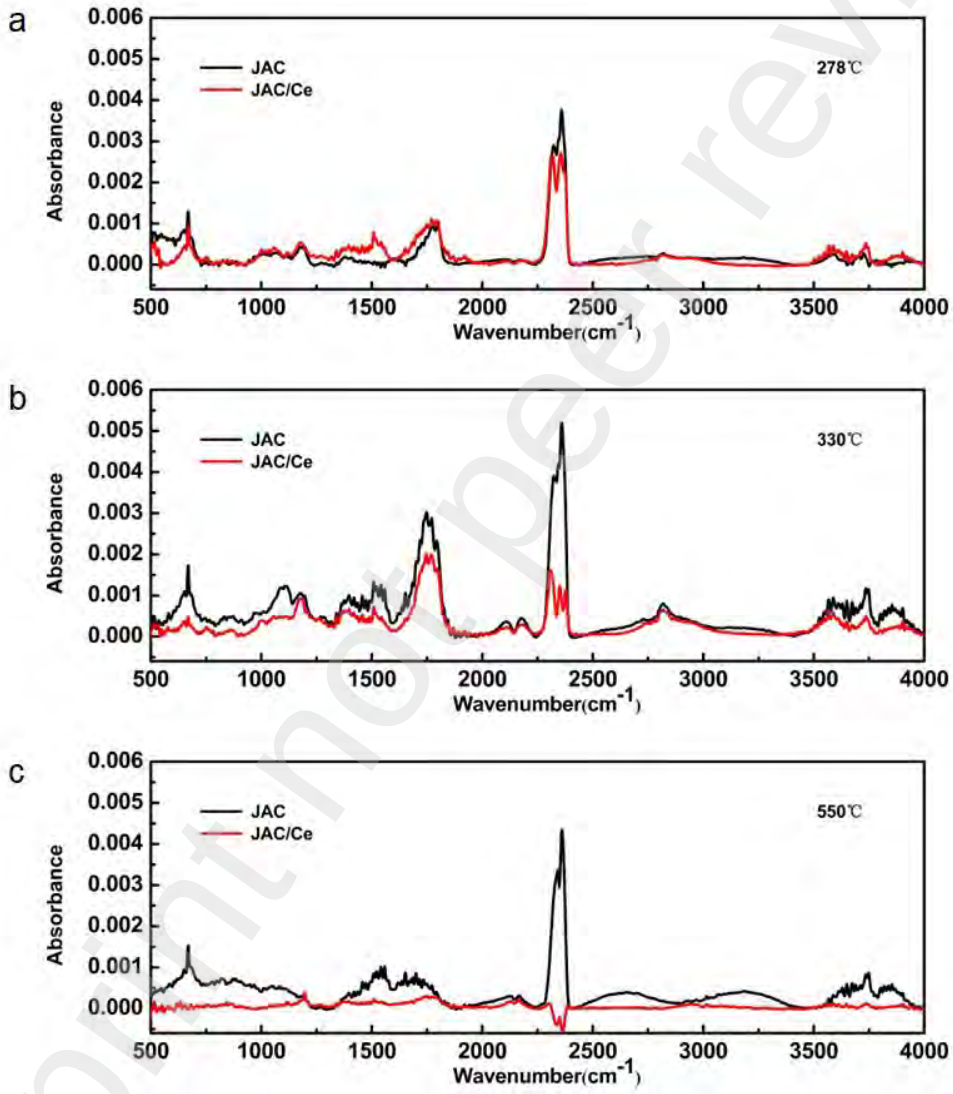

Fig. 2. TG-FTIR spectra of JAC and JAC/Ce pyrolysis at different pyrolysis temperatures: 278 ℃ (a), 330 ℃ (b), and 550 ℃ (c).

3.3 Electrochemical characterization

The electrochemical catalytic capacity of the JAC/Ce-BCs modified gold electrode to H_2O_2 were determined by cyclic voltammetry (CV). Fig. 3 showed the CV curves of the electrode modified with JAC/Ce-BC 400, JAC/Ce-BC 600 and JAC/Ce-BC 800. It could be found that compared with pure Au electrode, JAC/Ce-BC significantly improved the electrocatalytic capacity of H_2O_2, which indicated that JAC/Ce-BC had the potential to improve the performance of electrochemical sensors [30]. The CV current of JAC/Ce-BC modified electrode increased with the increase of pyrolysis temperature. However, the modification effect of JAC/Ce-BC 400 composite was almost the same as that of pure Au, and there was no obvious improvement effect. It was also found that the oxidation performance of electrodes modified with JAC/Ce-BC 800 composite was much better than JAC/Ce-BC 600. Therefore the 600 and 800 ℃ were selected as the two main pyrolysis temperatures to find out why the electrochemical performance of JAC/Ce-BC 600 was not satisfactory compared with JAC/Ce-BC 800.

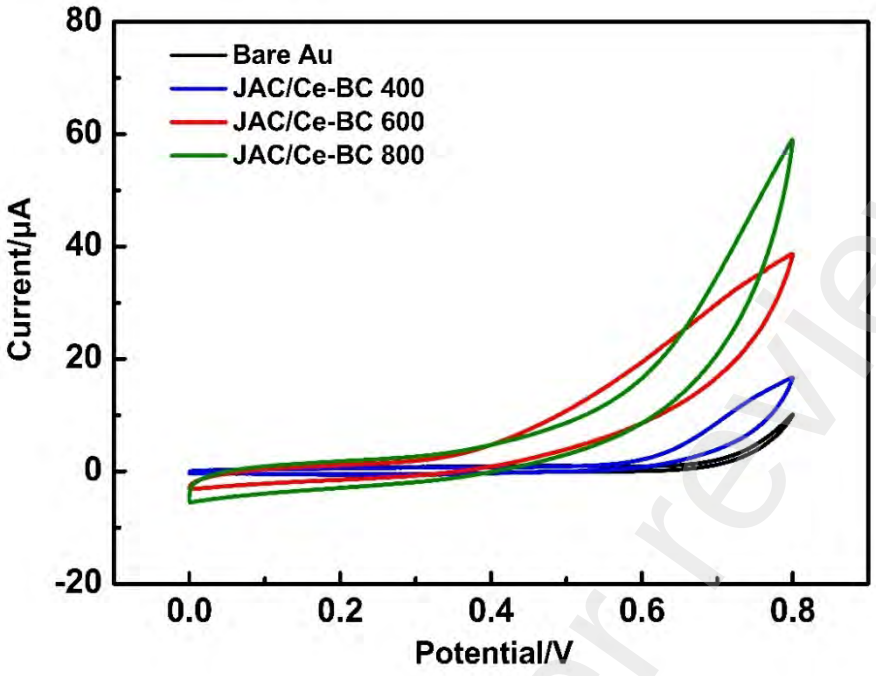

Fig. 3. CV curves for H_2O_2 of the electrode modified with JAC/Ce-BC composites derived from pyrolysis at 400, 600, and 800 ℃.

3.4 Physical structure

The SEM image of the natural JAC in Fig. 4(a) showed that the surface of the natural JAC was porous and smooth. After carbonization, it was obvious that JAC-BC 600 and JAC-BC 800 still retain the structure of JAC, as shown in Fig. 4 (b) and (c). Through comparison, it could also be found that the aperture of JAC-BC 800 was larger than JAC-BC 600, which had a certain promoting effect on electrochemical detection. Fig. 4(d) and (e) showed that JAC/Ce-BC possessed a rough surface and porous structure. However, with the pyrolysis temperature increasing from 600 to 800 ℃, the pore diameter decreased, forming more pores at 800 ℃. The EDS (Fig. 4f) elemental maps revealed that the compositional distributions of three elements (C, O, and Ce) in the JAC/Ce-BC were uniform. Ce

was evenly distributed on the surface of JAC/Ce-BC, indicating that Ce had been successfully loaded. Given our previous work [18], the different treatment methods result in structural differences.

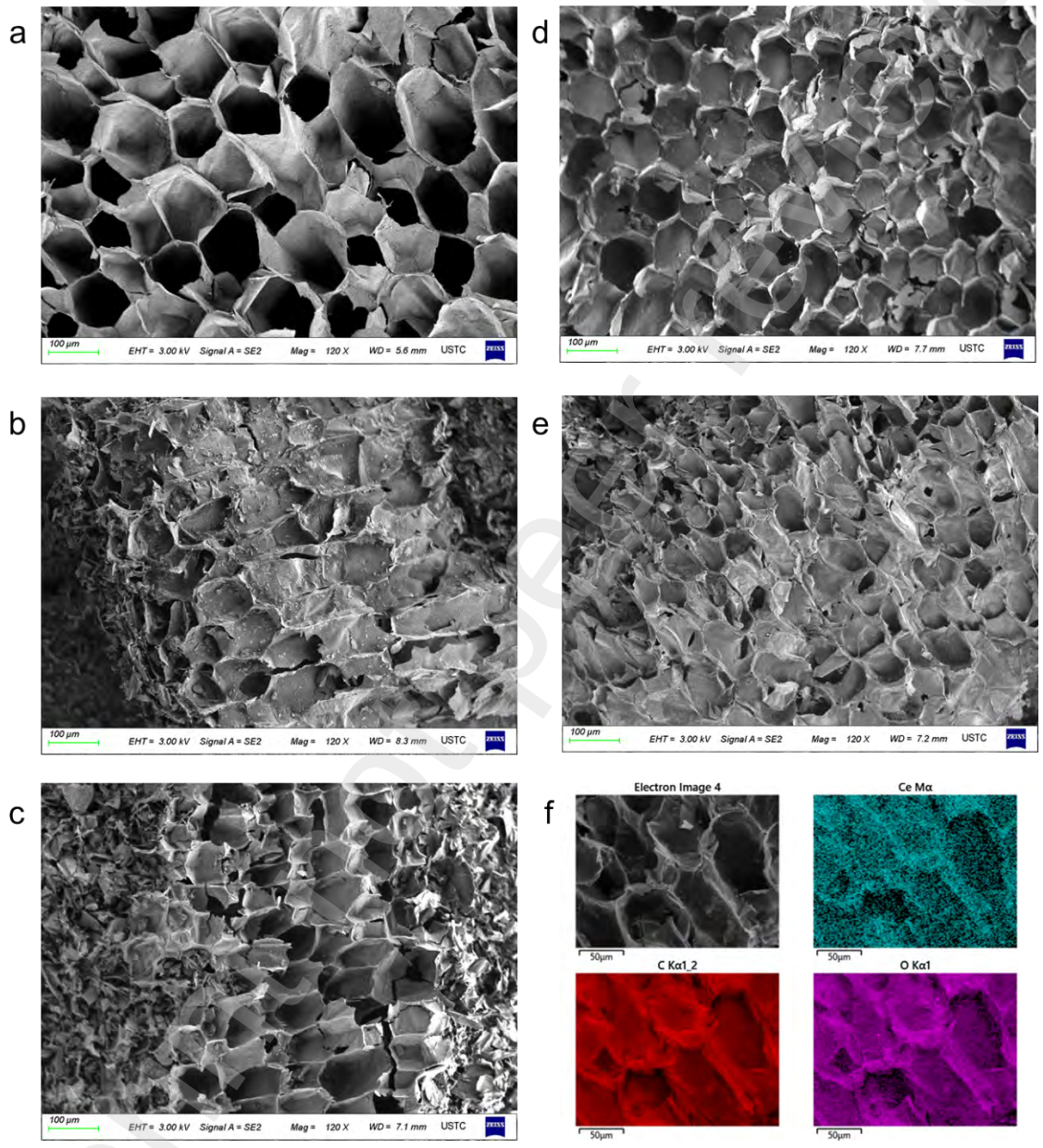

Fig. 4. SEM image of natural JAC (a), JAC-BC 600 (b), JAC-BC 800 (c), JAC/Ce-BC 600 (d) and JAC/Ce-BC 800 (e). EDS mapping of JAC/Ce-BC 800 (f).

To better understand the chemical structures of these materials in-depth, detailed chemical state analysis was performed, including XRD, Raman spectroscopy, and XPS. JAC/Ce-BC exhibited 5

peaks at 28.6°, 33.1°, 47.4°, 56.3°, and 59.0°, respectively, which could be assigned to (111), (200), (220), (311) and (222), corresponding to the fluorite-like structure of cerium oxide nanocrystals [31] (Fig. 5a). The crystalline size of the nanostructured cerium oxide could be calculated based on the Sherrer equation according to the main peak of (111) located at 28.6°. JAC/Ce-BC 800 exhibited a crystallite size of 7.6 nm with an interplanar spacing of 0.311 nm, corresponding to the *d* spacings from the (111) plane. JAC/Ce-BC 600 did not exhibit a typical fluorite-like cerium oxide structure due to the impurity peaks. It could be caused by incomplete transformation from cerium nitrate precursors to nanostructured cerium oxide [32].

Raman spectra of JAC-BC and JAC/Ce-BC were shown in Fig. 5b D peak at 1330 cm^{-1} represented disordered non-crystalline carbon like sp^3C, which arised from defects and amorphous species. G peak at 1580 cm^{-1} was on behalf of graphite carbon originating from in-plane vibration of sp^2 carbon related to the ordered carbon species, for example, C=C. The intensity ratio I_D/I_G illustrated the graphite degree and defective nature of carbon-based materials. The I_D/I_G value of JAC/Ce-BC 800 (1.0195) was higher than that of JAC/Ce-BC 600 (0.882), which meant more defectives were formed and more porous biochar was generated as the increase of temperature. It further confirmed the XRD observation of cerium oxide formation since the existence of cerium oxide made graphite sheets of biochar more oxidized and disordered.

The chemical composition and the elemental analysis were analyzed by X-ray photoelectron spectroscopy (XPS). As shown in the survey spectra (Fig. 5c), the peaks of the C 1*s* and O 1*s* could be identified since JAC-BC and JAC/Ce-BC were both porous carbon materials. Moreover, the peaks of Ce 3*d* shown in the survey spectra of JAC/Ce-BC composites confirmed Ce's existence. A certain amount of chlorine (~200 eV), calcium (~348 eV), and potassium (~379 eV) elements were observed

from the survey spectra due to the composition of the biomass. However, these impurities existed in trace amounts and thus would not be taken into discussion. Table 2 showed the elemental composition in terms of their atomic percentages. When increasing the pyrolysis temperature from 600 to 800 ℃, there was a significant decrease in oxygen content either with or without the presence of Ce. The oxygen species could be attributed to certain surface functional groups attached to the biochar and adsorbed moisture [33]. Less than 1% of nitrogen was observed for all analyzed samples, which could be attributed to the residues from the biomass and the nitrogen atmosphere during pyrolysis. None of the JAC/Ce-BC samples treated at 600 and 800 ℃ showed an increased amount of nitrogen species, further confirming the complete decomposition of cerium nitrate incorporated into the JAC during immersion pretreatment. Both JAC/Ce-BC 600 and JAC/Ce-BC 800 retained less than 1% of Ce species, varying from 0.7% to 0.3%, while JAC/Ce-BC 800 showed an apparent lower amount of Ce compared with JAC/Ce-BC 600. It needed to be noted that the measured quantities were below the instrumental resolution to draw a satisfactory conclusion about the absolute comparison. On the other hand, the decreased amount of Ce species in JAC/Ce-BC 800 might also result from Ce incorporation into the carbonaceous layers. The chemical state of carbon and oxygen of the synthesized biochar materials and the oxidation states of Ce was further examined by XPS. As shown in Fig. 5d, nanostructured cerium oxide in JAC/Ce-BC 600 and JAC/Ce-BC 800 existed as a mixture of Ce^{3+}/Ce^{4+} states with Ce^{4+} as the dominant species, as reported mostly for nanostructure cerium oxide materials. The Ce^{3+} concentration of biochar synthesized at 600 and 800 ℃ were 7 (±5) % and 4 (±5) %, respectively, which did not have any significant correlation with pyrolysis temperature from a statistical point of view. The Ce^{3+}/Ce^{4+} served as the active site since the quick switch between Ce^{3+}/Ce^{4+} oxidation states had been reported to participate in many catalytic reactions [34]. The O 1*s*

spectra of measured samples showed a typical mixed oxygen species of carbon-based biomaterials with a broadened peak around 532 eV (Fig. 5e). Detailed fitting of O 1*s* peak revealed four main peaks assigned to biochar: peak at 531.2 eV could be assigned to O-H related groups; peak at 532.1 eV assigned to C=O as ester or carboxyl related functional groups; peak at 533.4 eV further confirmed the presence of ester groups since it was usually assigned to O=C-O-R. A negligible peak at 535.3 eV could be assigned to bridging oxygen connected with phenyl groups, which was understandable due to the organic compound existed in the raw material. For JAC/Ce-BC pyrolyzed at different temperature, a clear shoulder around 530 eV was observed for the Ce containing JAC/Ce-BC, which was assigned to the lattice oxygen of cerium oxide. It further confirmed the existence of nanostructured cerium oxide incorporated into the matrix. Fig. 5f showed the fitted C 1*s* spectra of all measured samples. All spectra showed four components: C-C at 284.7 eV, C-OH at 285.7 eV, C-O at 288.0 eV, and COOH around 290.0 eV. As the increase of pyrolysis temperature from 600 to 800 ℃, the COOH peak decreased and almost disappeared, indicating the complete pyrolysis process generating gaseous products (such as CO_2), which further contributed to the porous morphological structure of the biochars.

With all the information obtained from the physicochemical analysis of the synthesized materials, we can summarize the decomposition/pyrolysis mechanism of using JAC/Ce to produce cerium contained biochar. It was confirmed from both XRD and XPS analysis that nanostructured cerium oxide was formed during the pyrolysis over 600 ℃, while a higher temperature up to 800 ℃ resulted in a complete hydrothermal transformation of cerium oxide crystallite structure in the size of ~7 nm. During the pyrolysis process, cerium oxide, in turn, catalyzed the reaction and accelerated the decomposition rate. The production of volatile compounds contributed to the porous morphology of

the biochar produced from these Jerusalem artichoke straw cores. The produced nanostructured cerium oxide tends to locate at the surface of the biochar support, providing potentially promising materials as cerium oxide doped biochar nanocomposites.

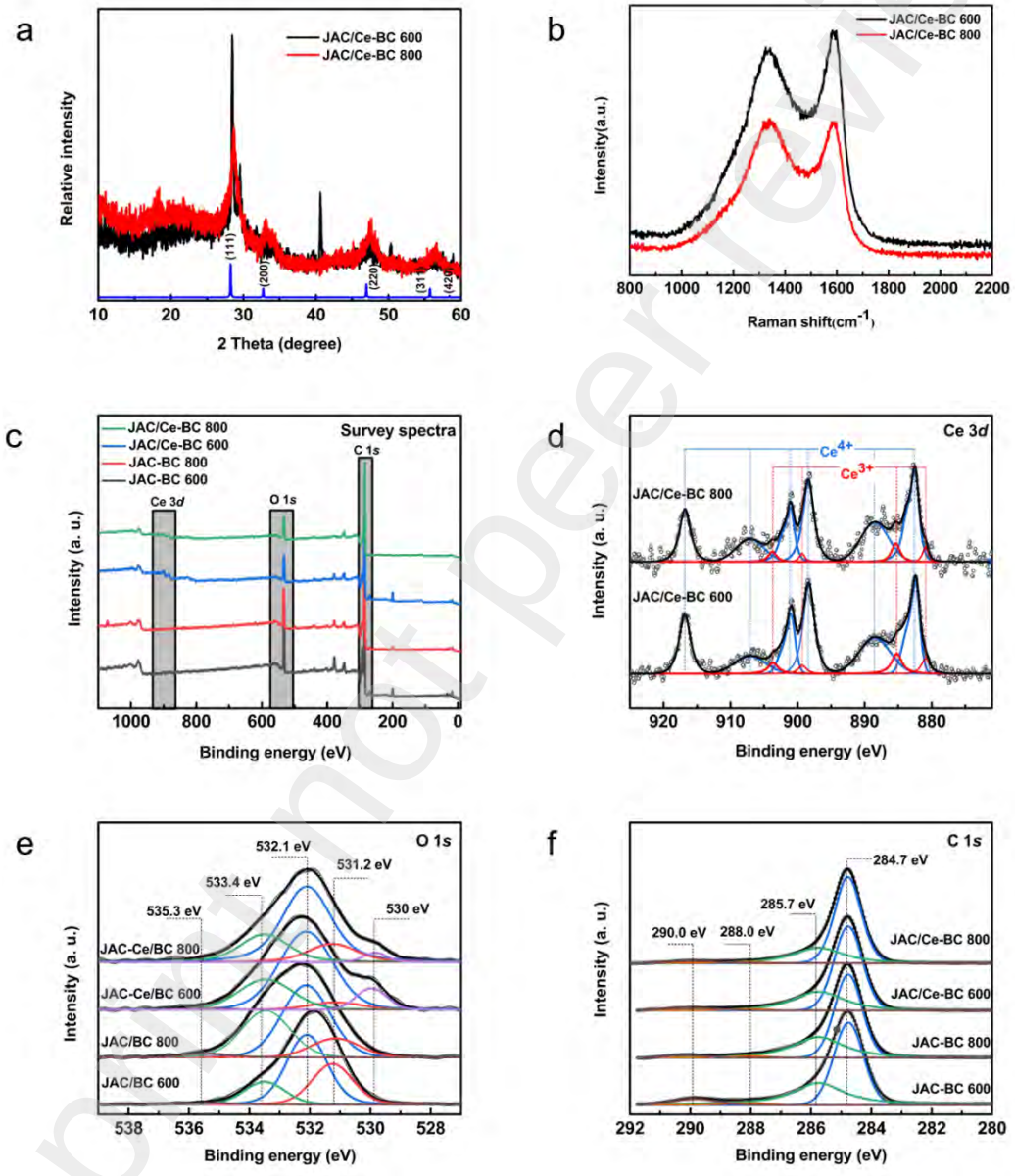

Fig. 5. XRD patterns of JAC/Ce-BC 600 and JAC/Ce-BC 800 (a), Raman spectra of JAC/Ce-BC 600 and JAC/Ce-BC 800 (b), Elemental analysis by XPS survey spectra (c); Ce 3*d* spectra (d); O 1*s* spectra (e); C 1*s* spectra (f).

Table 2 The atomic percentage of C, O, N, and Ce by XPS analysis.

Atomic percentage (%)	C	O	N	Ce	total
JAC-BC 600	76.9	22.3	0.9	N/A	100
JAC-BC 800	82.0	17.4	0.7	N/A	100
JAC/Ce-BC 600	85.2	13.5	0.6	0.7	100
JAC/Ce-BC 800	88.7	10.6	0.4	0.3	100

4. Conclusion

The pyrolysis behavior of JAC and JAC/Ce were studied by TG-FTIR. TG results showed that the addition of cerium nitrate reduced the pyrolysis temperature and accelerated the pyrolysis process of JAC. FTIR analysis revealed that H_2O, CO_2, CO, CH_4, C-O, C=O and aromatic C=C were released during the pyrolysis. Cerium oxide doped biochar composites were prepared and the electrochemical characteristics and physical structures were analyzed. JAC/Ce-BC 800 showed improvement in electrochemical performance compared with JAC/Ce-BC 600. Nanostructured cerium oxide was observed during the pyrolysis process, with an ordered crystalline structure less than 10 nm and a dominant Ce^{4+} oxidation state. The improved electrocatalytic capacity of JAC/Ce-BC 800 could be attributed to cerium oxide formation on the surface of the biochar facilitating the electron transfer process through the switch between the Ce^{3+}/Ce^{4+} oxidation states. It was concluded that such cerium oxide doped biochar composites had great potential in electrochemical applications.

Acknowledgments

This study was supported the National Natural Science Foundation of China (31901406).

Reference

[1] R.K. Mishra, Q. Lu and K. Mohanty, J. Anal. Appl. Pyrolysis., 150, (2020) 104887.
[2] M.A. Mehmood, M.S. Ahmad, Q. Liu, C.G. Liu, M.H. Tahir, A.A. Aloqbi, N.I. Tarbiah, H.M. Alsufiani and M. Gull, Energy. Conv. Manag., 194, (2019) 37.
[3] M.R. Cabral, E.Y. Nakanishi, G. Marmol, J. Palacios, S. Godbout, R. Lagace, H. Savastano and J. Fiorelli, Ind. Crop. Prod., 122, (2018) 214.
[4] S.Q. Lv, R.X. Wang, Y.M. Xiao, F.C. Li, Y.W. Mu, Y. Lu, W.T. Gao, B. Yang, Y.X. Kou, J. Zeng and C.M. Zhao, Ind. Crop. Prod., 134, (2019) 71.
[5] S. Rasam, A.M. Haghighi, K. Azizi, A. Soria-Verdugo and M.K. Moraveji, Fuel, 280, (2020) 118665.
[6] B. Wang, F.F. Xu, P.J. Zong, J.H. Zhang, Y.Y. Tian and Y.Y. Qiao, Renew. Energy., 132, (2019) 486.
[7] L. Yan, Y. Liu, Y. Zhang, S. Liu, C. Wang, W. Chen, C. Liu, Z. Chen and Y. Zhang, Bioresour. Technol., 297, (2020) 122381.
[8] Q. Shen, Z. Wang, Q. Yu, Y. Cheng, Z. Liu, T. Zhang and S. Zhou, Environ. Res., 183, (2020) 109195.
[9] M.Z. Xue, H. Xu, Y. Tan, C. Chen, B. Li and C.M. Zhang, J. Electroanal. Chem., 893, (2021) 115306.
[10] J.-F. Cai, J. Fan, X.-S. Liu, K. Sun, W. Wang, M.-X. Zhang, H.-L. Li, H.-F. Xu, W.-J. Kong and F.-H. Yu, Sci. Total. Environ., 788, (2021) 147707.
[11] F.Y. Jiang, Y.H. Zhou, R. Chen, T.T. Liu, J.Y. Luo and Y.B. Huang, Appl. Surf. Sci., 560, (2021) 150039.
[12] Y.F. Feng, H.Y. Lu, Y. Liu, L.H. Xue, D.D. Dionysiou, L.Z. Yang and B.S. Xing, Chemosphere, 185, (2017) 816.
[13] A. Khataee, P. Gholami, D. Kalderis, E. Pachatouridou and M. Konsolakis, Ultrason. Sonochem., 41, (2018) 503.
[14] D. Bao, Z. Li, R. Tang, C. Wan, C. Zhang, X. Tan and X. Liu, J. Environ. Manage., 284, (2021) 112113.
[15] L. Liu, G. Deng and X. Shi, Sci. Rep., 10, (2020) 5149.
[16] Y. Zhu, B.J. Yi, H.Y. Hu, Z.X. Zong, M.J. Chen and Q.X. Yuan, J. Environ. Chem. Eng., 8, (2020) 104112.
[17] R.H. Li, H. Huang, J.J. Wang, W. Liang, P.C. Gao, Z.Q. Zhang, R. Xiao, B.Y. Zhou and X.F. Zhang, J. Clean. Prod., 216, (2019) 25.
[18] Y. Bi, L. Ye, Y. Mao, L. Wang, H. Qu, J. Liu and L. Zheng, Biosens. Bioelectron., 140, (2019) 111271.
[19] H.Y. Guo, L.J. Ma, F. Shen, G. Yang, Y.Z. Zhang, S.H. Deng, J. Zhang, C. Song and Y.M. Zeng, J. Rare. Earths., 35, (2017) 593.
[20] L. Ye, R. Wang, G. Ji, H. Wu, H. Qu, L. Wang and J. Liu, Energy. Res., 45, (2020) 8083
[21] S. Ceylan and J.L. Goldfarb, Energy. Convers. Manag., 101, (2015) 263.

[22] J. Cao, G. Xiao, X. Xu, D. Shen and B. Jin, Fuel. Process. Technol., 106, (2013) 41.
[23] T. Xu and X. Huang, Fuel., 89, (2010) 2185.
[24] Z. Luo, S. Wang and X. Guo, J. Anal. Appl. Pyrolysis., 95, (2012) 112.
[25] Z. Ni, H. Bi, C. Jiang, H. Sun, W. Zhou, Z. Qiu and Q. Lin, Fuel., 320, (2022) 123960.
[26] C. Wang, H. Bi, Q. Lin, X. Jiang and C. Jiang, Renew. Energy., 160, (2020) 1048.
[27] Z. Ni, H. Bi, C. Jiang, J. Tian, H. Sun, W. Zhou and Q. Lin, Sci. Total. Environ., 804, (2022) 150217.
[28] P. Lu, L. Ye, X. Yan, X. Chen, P. Fang, D. Chen, D. Chen and C. Cen, Appl. Surf. Sci., 600, (2022) 154161.
[29] L. Tao, X. Ma, L. Ye, J. Jia, L. Wang, P. Ma and J. Liu, J. Anal. Appl. Pyrolysis., 158, (2021) 105267.
[30] H. Yuan, Y. Zhao, J. Yang, C. Xiong, D. Li and Y. Chen, J. Anal. Appl. Pyrolysis., 166, (2022) 105606.
[31] X. Li, P. Liu, W. Chen, Y. Wu, T. Lei, S. Huang, Y. Li, S. Wu and Z. Wang, J. Anal. Appl. Pyrolysis., 162, (2022) 105436.
[32] K. Nusrath and K. Muraleedharan, J. Anal. Appl. Pyrolysis., 120, (2016) 379.
[33] Q. Cao, T. An, J. Xie, Y. Liu, L. Xing, X. Ling and C. Chen, J. Anal. Appl. Pyrolysis., 166, (2022) 105590.
[34] H. Zhou, M.A. Akhtar, Y. Wan, K. Ding, R. Ruan, H. Zhang and S. Zhang, J. Anal. Appl. Pyrolysis., 152, (2020) 104973.